Journal of Alloys and Compounds 502 (2010) 279–282

Contents lists available at ScienceDirect

Journal of Alloys and Compounds

journal homepage: www.elsevier.com/locate/jallcom

Rietveld analysis and Mössbauer spectroscopy studies of nanocrystalline hematite α-Fe_2O_3

O.M. Lemine[a,*], M. Sajieddine[b], M. Bououdina[c], R. Msalam[d], S. Mufti[d], A. Alyamani[e]

[a] Department of Physics, College of Sciences, Imam University, Riyadh, Saudi Arabia
[b] Laboratoire de Physique et Mécanique des Matériaux, Sultan Moulay Slimane University, Béni-Mellal, Morocco
[c] Department of Physics, College of Science, University of Bahrain, Bahrain
[d] Radiation Technology Center, KACST, Riyadh, Saudi Arabia
[e] National Nanotechnology Research Centre, KACST, Riyadh, Saudi Arabia

ARTICLE INFO

Article history:
Received 9 March 2010
Received in revised form 9 April 2010
Accepted 24 April 2010
Available online 5 May 2010

Keywords:
Nanoparticles
Hematite
Ball milling
Mössbauer
X-ray diffraction
Rietveld

ABSTRACT

The effect of high energy ball milling on the hematite for milling periods of times ranging from 1 to 48 h was investigated by Rietveld analysis based on XRD patterns and Mössbauer spectroscopy. An expansion of the unit cell parameters was observed. Both Scherrer method and Rietveld analysis show an evident decrease of the grain size with the increase of the milling time. Moreover, some dependence of the lattice parameters on the grain size was observed. Mössbauer spectroscopy measurements reveal that there are two kinds of particles which co-exist in the sample: nanostructured and micrometric hematite. The magnetic hyperfine field is affected by the grain size.

1. Introduction

In recent years, nanoparticle systems have attracted increasing attention due to their immense technological applications [1,2]. Many nanoparticle systems have been investigated particularly the magnetic nanoparticles in the field of nanoscience and nanotechnology, because of the unique and novel physico-chemical properties that can be attained according to their size, morphology and engineering form [3–5]. Hematite nanoparticles (α-Fe_2O_3) have potential applications into many areas such as magnetism, catalysis, electrochemistry, and biotechnology. Several groups have been interested by the mechanical alloying of hematite [6–9]. Zduji et al. [16] studied the mechanochemical treatment of α-Fe_2O_3 powder in air and oxygen atmospheres using a conventional planetary ball mill. They observed that α-Fe_2O_3 completely transforms to Fe_3O_4, and for prolonged milling to the $Fe_{1-x}O$ phase, either in air or oxygen atmosphere. The transformation of α-Fe_2O_3 to Fe_3O_4 on wet-milling α-Fe_2O_3 under low milling energy conditions in vacuum was investigated by Campbell et al. [15]. Randrianantoandro et al. [6] studied the phase transformation from hematite to maghemite during high energy ball milling in ethanol. They show that maghemite (γ-Fe_2O_3) can be directly produced from hematite (α-Fe_2O_3) after 48 h milling time. Recently, we studied the synthesis and structural characterization of hematite nanoparticles produced by dry mechanical alloying [11,17].

In this report, the effect of ball milling time on the hematite was investigated. Structure (phase formation) and microstructural parameters (crystallite size) evolution were analysed by means of Rietveld analysis. Magnetic properties were measured and analysed by means of Mössbauer spectroscopy measurements.

2. Experimental

Commercial α-Fe_2O_3 powder was used as the starting material. The mechanical milling was carried out in a planetary ball mill Fritsch Pulverisette 6. The powder was ground in vial with 200 g of mixture 1:1 in weight of stainless steel balls (10 and 15 mm in diameter). Different milling times were used (1, 6, 12, 24 and 48 h) and the sample to balls weight ratio was fixed to 1:10 and the milling intensity was fixed to 250 rpm. X-ray diffraction (XRD) measurements were performed using Shimadzu diffractometer (θ–2θ) by using Cu-Kα radiation (λ = 1.5418 Å). Qualitative and quantitative analyses were carried by the Rietveld method using Rietan's programme [12]. Both refined lattice parameters and the crystallite size were reported.

The crystalline size was also calculated using Schererrer formula:

$$D = \frac{K\lambda}{B\cos\theta} \quad (1)$$

In this case, the peak width B (in rad) was determined as full width at half-maximum (FWHM) by a Gaussian fitting.

^{57}Fe Mössbauer spectroscopy provided relevant information concerning the valence state of iron atoms and magnetic hyperfine characteristic of iron oxide

* Corresponding author.
E-mail address: leminej@yahoo.com (O.M. Lemine).

0925-8388/$ – see front matter © 2010 Elsevier B.V. All rights reserved.
doi:10.1016/j.jallcom.2010.04.175

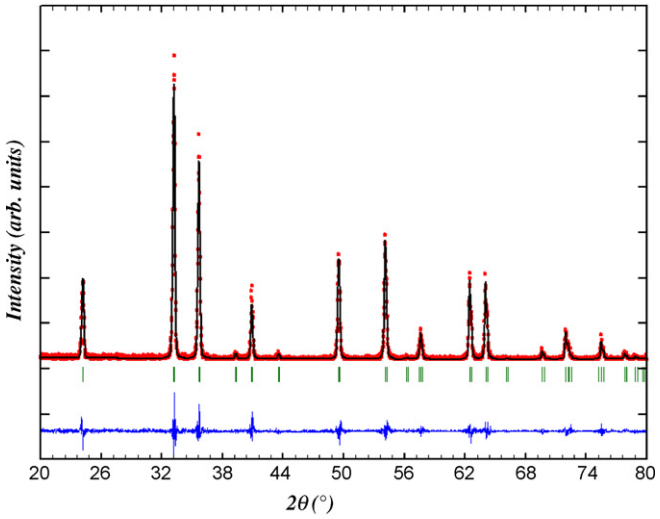

Fig. 1. An example of pattern fitting using Rietveled refinements. The net difference between the observed and measured profile is given on the bottom of the plot.

phases present in the obtained nanoparticles. Mössbauer spectra are recorded at room temperature in the standard transmission geometry, using a constant acceleration signal spectrometer with Co^{57} source diffused into a rhodium matrix. Hyperfine interaction parameters were derived from the Mössbauer spectra using a least-squares method. Isomer shifts are referred to α-Fe at room temperature.

3. Results and discussion

XRD characterization of the samples was described in our previous work [11,17], but brief description is reported here. All Bragg peaks of the XRD patterns showed only the hematite reflections, indicating that there is no change of the main phase, hematite α-Fe_2O_3, during the milling. With increasing the milling time, the diffraction peaks became broader and their relative intensity decreases due the particle size reduction and accumulation of strains and defects during the milling process. Qualitative and quantitative phase analyses using the Rietveld method have been performed based on the XRD patterns. An example of pattern fitting after refinements is shown in Fig. 1. During the refinements, the zero shift and the instrumental parameters were determined using a standard (Si 640 b) and then fixed during the refinement of all the samples. There are several parameters for the evaluation of pattern fitness. One of the common parameters is the goodness-of-fit indicator S, which is defined by: $S = R_{wp}/R_e$, where R_{wp} and

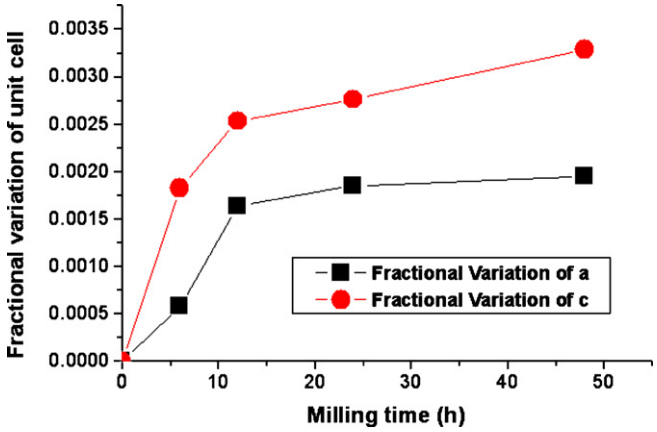

Fig. 3. Evolution of the fractional unit cell parameters (a and c) for different milling times.

R_e, are respectively the R-weighted and the R-expected patterns [13]. Table 1 presents the results of the Rietveld refinements for the samples as function of the milling time. It can be seen that the lattices parameters increase for longer milling times, while the crystallite size decreases. Similar behavior has been reported by several groups where a clear reduction of the grain size for longer milling times has been observed [9,10,14]. The decrease of the crystallite size with increasing the milling time has been also confirmed by Sherrer's formula (Table 1) but the crystallite sizes obtained by Scherrer's formula are slightly higher than those obtained earlier by the Rietveld analysis (Fig. 2). This difference may be due to the fact that the effect of the internal strain is not considered in Scherrer model, where the peak shape is fitted with a Gaussian only. However, in the Rietveld method, the peaks shape profile is fitted using a Voight function, which is a combination of both Gaussian (crystallite size) and a Lorentzian (microstrain) functions.

Fig. 3 shows the fractional variation of unit cell parameters:

$$\frac{\Delta a}{a_0} = \frac{a - a_0}{a_0} \tag{2}$$

and

$$\frac{\Delta c}{c_0} = \frac{c - c_0}{c_0} \tag{3}$$

where a_0 and c_0 are the unit cell parameters for the non-milled sample, whereas a and c are the unit cell parameters of the hematite during milling [10,14]. It is shown from Fig. 3 that the quanti-

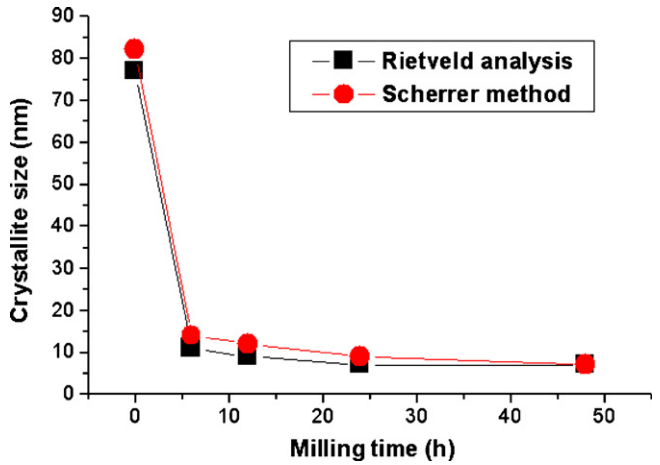

Fig. 2. Comparison of the evolution of the crystallite size between the Rietveld analysis and Scherrer's method with milling time.

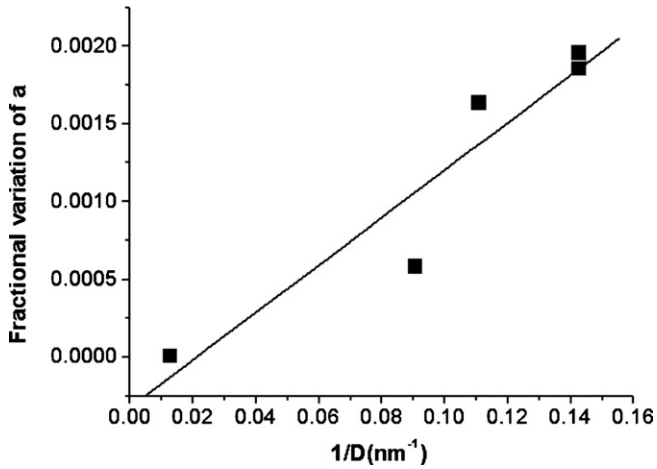

Fig. 4. Fractional variation of the lattice parameter a versus the inverse of the average grain size D.

Table 1
Rietveld analysis refinements results and crystallite size estimated using Scherrer's method for various milling times.

Milling time (h)	Rietveld analysis		Scherrer's method	
	Lattice parameter *a* (Å)	Lattice parameter *c* (Å)	Crystallite size (nm)	Crystallite size (nm)
0	5.0328	13.7447	77	82
6	5.0357	13.7698	11	14
12	5.0410	13.7795	9	12
24	5.0421	13.7826	7	9
48	5.0426	13.7898	7	7

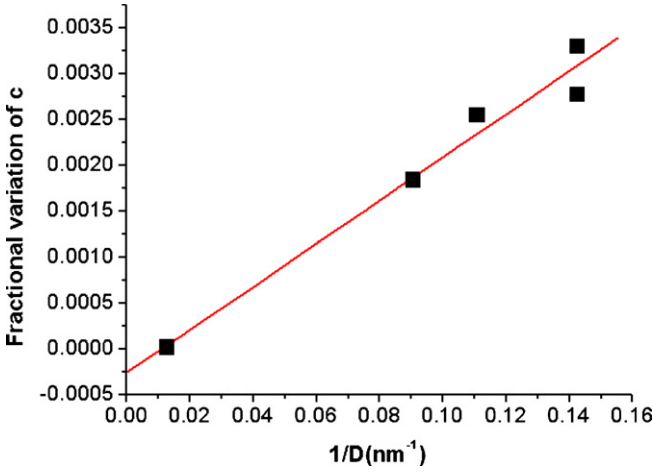

Fig. 5. Fractional variation of the lattice parameter *c* versus the inverse of the average grain size *D*.

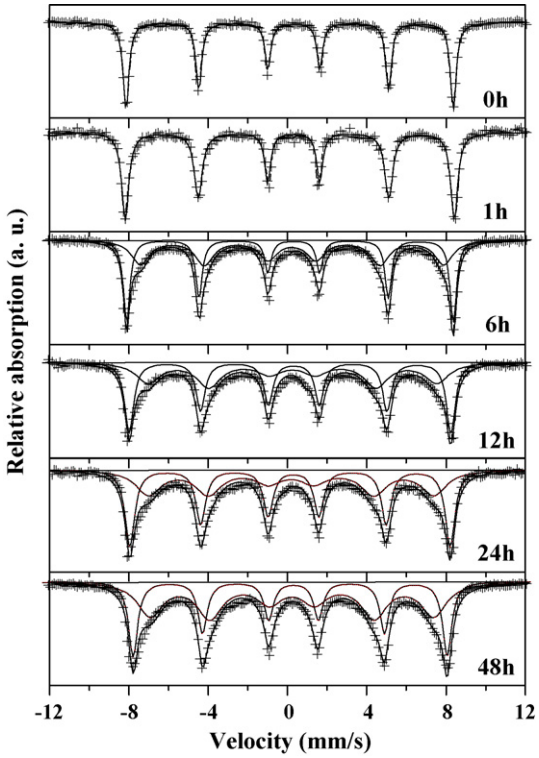

Fig. 6. Mössbauer spectra at room temperature for different milling times.

ties $\Delta a/a_0$ and $\Delta c/c_0$ are both positive for all milled samples and increase with increasing the milling time, indicating the presence of an anisotropic lattice expansion. Others groups obtained the same results for the hematite milled under air and in ethanol [10,14].

Figs. 4 and 5 show the evolution of the fractional variation of unit cell parameters with the inverse of the average calculated crystallite size. It is clear that there is some dependence of the lattice parameters and the crystallite size. The unit cell increases as the crystallite size decreases. Stewart et al. [14] found that for short milling time, the lattice parameters of the hematite increase with the decrease of the size of the particles. However, they have questioned about the possibility to observe the same behavior at prolonged milling time. According to the results reported here, similar results, i.e., crystallize size reduction for longer milling time, are observed (Fig. 2).

Fig. 6 shows the room-temperature transmission Mössbauer spectra of the samples obtained for different milling times. Table 2 gives the results of the spectra fitting. The spectrum for the non-milled sample was adjusted by introducing only one sextet with hyperfine field (B_{hyp}) of 51.3 T, quadrupolar shift of −0.2 mm/s and isomershift of 0.37 mm/s relative to α-Fe. From these values, we conclude that the initial powder consists only of α-Fe_2O_3 crystalline phase. When the milling time increases, the spectra exhibit some line broadening and the intensity of the initial lines decreases. The best fit was obtained by considering a new sextet. The new component might be attributed to the hematite nanoparticles and the first sextet is associated to the micrometric hematite. It can be seen that the decrease of the relative abundance of the micrometric component (first sextet) with milling times is accompanied by the increase of the nanometric component (second sextet). The increase of the new component is in accordance with the hypothesis that the disordered regions become apparent as the grain size reduces [14]. It is also noticed that the B_{hyp} of the new component decrease (Fig. 7a) while the B_{hyp} of the other sextet approaches always at the value of the bulk hematite (Fig. 7b).

This result can be explained by the dynamic effects. Small grains produced upon applying prolonged milling are basically single

Table 2
Results of the Mössbauer analysis spectra fitting for various milling times.

Milling times (h)	First sextet			Second sextet		
	B_{hyp} (kOe)	IS (mm/s)	Relative area (%)	B_{hyp} (kOe)	IS (mm/s)	Relative area (%)
0	513.4	0.36	100	–	–	0
1	515.8	0.36	100	–	–	0
6	512.2	0.37	48	475.7	0.382	52
12	504.5	0.37	52	452.7	0.4	48
24	502.2	0.36	52	447.7	0.34	48
48	492.2	0.37	40	444	0.37	60

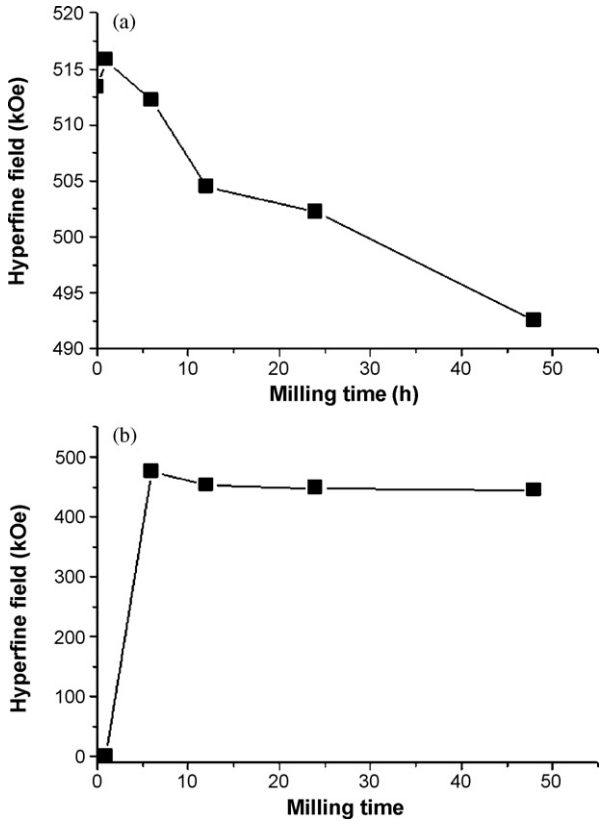

Fig. 7. Evolution of the hyperfine field with the milling time for the hematite phase (a) nanometric and (b) micrometric.

crystals and single magnetic domains. The magnetic interaction between such particles is weak even for tightly pressed powder as magnetic domains remain antiferromagnetic (or very weakly ferromagnetic below Morin transition). Hence, the relaxation of the domain magnetization can occur even at room temperature. Such process leads to the reduction of the magnetic dipole interaction between nucleus and the electronic shell and produces significant line broadening, the latter depending on the particular hyperfine line. Strong compaction of the powder prevents observation of the completely collapsed magnetic hyperfine structure easily seen for hematite particles really dispersed in the non-magnetic carrier. In addition, the dynamic effect hypothesis seems supported by the constancy of the overall shift (isomer shift) versus milling time. It means that the electron density on the iron nucleus remains almost unchanged during milling. On the other hand mixed state is observed around mixed state is observed around Morin transition, i.e., regions of either antiferromagnetic order or with the canted structure, as the Morin transition is driven by defects. One can vary Morin transition temperature applying pressure or external field. Usually Morin transition temperature is lowered by extensive defects, i.e., for nanoparticles.

The results reported here are in good agreement with those reported in the literature [6,9,14]. Sancheza et al. [10] obtained only nanoparticles and micorparticles of α-Fe_2O_3 by performing milling in ethanol. When milling under air, the authors detected a new phase (maghmite). The difference with the results reported here may be explained by the experimental procedure and milling conditions. In the experimental conditions reported in this work, the bowls were closed during the milling, while in their experiments; the bowls were opened after every hour of milling. More importantly, their experimental conditions are somehow different compared to the conditions reported in this work: type of miller pulverisette P5 (P6); milling speed 390 rpm (250 rpm); balls/powder ratio 1:20 (1:10). Therefore, the phase transformation, hematite–maghmite occurs, as reported by the authors [10], due to the high milling intensity, the values of both milling speed and balls/powder ratio are much higher than the values reported in this work.

In order to clarify some points, such as how to distinguish between the two components, the Morin temperature evolution with milling time; Mössbauer measurements either at lower temperature or in the external field will be conducted.

4. Conclusion

The crystallite size decreases with increasing the milling to reach a nanometric size after 48 h of milling. The fractional variation of the unit cell parameters increases with the milling time, indicating the presence of an anisotropic lattice expansion. This anisotropic lattice dilation is correlated to both the decrease of the grain size and the increment of the structural disorder.

Mössbauer spectra show the existence of two components for the milled samples, one attributed to the nanocrystalline hematite and the second to micrometric hematite. The magnetic hypefine field and the relative abundances of each component are affected by the grain size.

Acknowledgment

This work was supported financially by King Abdulaziz City for Sciences and Technology (KACST).

References

[1] Q.A. Pankhurst, J. Conolly, S.K. Jones, J. Dobson, J. Phys. D: Appl. Phys. 36 (2003) R167.
[2] P. Moroz, S.K. Jones, B.N. Gray, Int. J. Hypertherm. 18 (2002) 267.
[3] G.A. Ozin, Adv. Mater. 4 (1992) 612.
[4] Y.S. Kang, S. Risbud, J.F. Rabolt, P. Stroeve, Chem. Mater. 8 (1996) 2209.
[5] M.P. Pileni, J. Phys. Chem. 105 (2001) 3358.
[6] N. Randrianantoandro, A.M. Mercier, M. Hervieu, J.M. Greneche, Mater. Lett. 47 (2001) 150.
[7] S. Bid, A. Banerjee, S. Kumar, S.K. Pradhan, Udayan De, D. Banerjee, J. Alloys Comp. 326 (2001) 292.
[8] M. Zdujic, C. Jovalekic, Lj. Karanovic, M. Mitric, D. Poleti, D. Skala, Mater. Sci. Eng. A 245 (1998) 109.
[9] M. Hofmann, S.J. Campbell, W.A. Kaczmarek, S. Welzel, J. Alloys Compd. 348 (2003) 278.
[10] L.C. Sancheza, J.D. Arboledaa, C. Saragovib, R.D. Zyslerc, C.A. Barreroa, Physica B 389 (2007) 145.
[11] O.M. Lemine, R. Msalam, S. Mufti, M. Sajieddine, A. Alyamani, Kh. Ziq, M. Bououdina, Int. J. Nanosci. 8 (3) (2009) 1.
[12] F. Izumi, in: R.A. Young (Ed.), The Rietveld Method, Oxford University Press, 1993 (Chapter 13).
[13] R.A. Young, in: R.A. Young (Ed.), The Riteveld Method, Oxford University Press, 1993 (Chapter 1).
[14] S.J. Stewarta, R.A. Borzib, E.D. Cabanillasc, G. Puntea, R.C. Mercadera, J. Magn. Magn. Mater. 260 (2003) 447.
[15] S.J. Campbell, W.A. Kaczmarek, G.-M. Wang, Nano-Struct. Mater. 6 (1995) 735.
[16] M. Zdujic, C. Jovalekic, Lj. Karanovic, M. Mitric, Mater. Sci. Eng. A 262 (1999) 204.
[17] O.M. Lemine, Superlattices Microst. 45 (2009) 576.